Exhibit IND23

Lindsey C. Blake, MD • William D. Robertson, MD • Cecil E. Hayes, PhD

Sacral Plexus: Optimal Imaging Planes for MR Assessment[1]

PURPOSE: To identify the optimal imaging planes for magnetic resonance (MR) evaluation of the sacral plexus (SP) and proximal sciatic nerve (SN).

MATERIALS AND METHODS: The SPs of 10 healthy adult volunteers were prospectively studied with T1-weighted MR imaging with custom-built pelvic phased-array coils. The conspicuity of 12 anatomic characteristics (comprising the SP and their relationship to normal pelvic anatomy) on a series of coronal, axial, and oblique images was graded. Results were evaluated with the Kruskal-Wallis and Wilcoxon signed rank tests.

RESULTS: At least two planes were necessary to assess the anatomy of the SP and SN. Analysis of average conspicuity scores showed that the direct coronal and direct axial planes were the best overall and were superior to other imaging planes in the demonstration of the L-4 and L-5 ventral rami, the lumbosacral trunk, the S-1 contribution to the SN, and the SN in the greater sciatic foramen. The sacral coronal plane was best for the visualization of the bony sacrum, sacral foramina, and proximal S-1 to S-4 nerve roots. The remaining imaging planes had limited utility.

CONCLUSION: MR imaging with a combination of direct coronal and direct axial planes enables thorough evaluation of all components of the SP and proximal SN.

THE sacral plexus (SP) and sciatic nerve (SN) are formed from contributions of the fourth lumbar through fourth sacral ventral nerve roots. The SP originates within the pelvis and gives rise to the SN, the largest nerve in the body, which exits the pelvis through the greater sciatic foramen (GSF) (Fig 1). The complex anatomy of this region and the diverse disease processes that may affect the SP are diagnostically challenging. Clinically, diseases affecting the SP and SN may result in disabling pain or morbidity. Furthermore, possible surgical management, operative technique, and the necessity for medical management depend on an accurate determination of the specific structures involved, including peripheral nerves. Until recently, it has not been possible to obtain detailed images of peripheral nerves. Technical advances in magnetic resonance (MR) imaging surface coils and pulse sequences have made detailed images of peripheral nerves possible based on the ability to accurately demonstrate normal and pathologic nerve morphology (1,2).

Computed tomography (CT) is an excellent imaging modality for visualizing most pelvic structures; however, CT has had limited success in demonstrating the detailed anatomy of the SP. It is possible that new spiral CT techniques may allow more accurate delineation of SP anatomy. Although the SN can be readily identified on axial CT images of the lower pelvis, the individual extradural L-4 to S-4 peripheral nerves that form the SP and SN cannot be reliably distinguished from normal adjacent intrapelvic soft tissues (3–5). MR imaging can depict individual peripheral nerves on the basis of their distinctive striated appearance (1), which differentiates them from adjacent musculoskeletal, lymphatic, and vascular structures. The purpose of this study was to identify the optimal MR imaging planes for demonstrating the SP and the proximal SN.

ANATOMY

The SP is formed by the ventral rami of L-4 to S-4. A variable-sized portion of the L-4 rami joins with L-5 to form an important structure, the lumbosacral trunk (LST). The LST is consistently found medial to the psoas muscle and enters the pelvis just anterior to the sacral ala, medial to the sacroiliac joint. As the LST enters the pelvis, it joins the S-1 ventral rami to form a larger upper band. The S-1 to S-4 rami enter the pelvis through the four paired sacral foramina. S-1 to S-2 are relatively larger than S-3 to S-4, which are distinctly smaller nerves. S-2 to S-4 join together to form a smaller inferior band (6).

The nerves of the SP have an inferior, posterior, and lateral course in the pelvis. SP nerve roots are located

Index terms: Magnetic resonance (MR), technology, 339.121411 • Nerves, sacral, 339.121411, 339.92 • Nerves, sciatic, 339.121411, 339.92

Abbreviations: GSF = greater sciatic foramen, LST = lumbosacral trunk, SN = sciatic nerve, SP = sacral plexus.

Radiology 1996; 199:767–772

[1] From the Department of Radiology, Box 357115, University of Washington, School of Medicine, 1959 NE Pacific St, Seattle, WA 98195. From the 1994 RSNA scientific assembly. Received December 5, 1995; revision requested January 15, 1996; revision received February 5; accepted February 12. Address reprint requests to W.D.R.

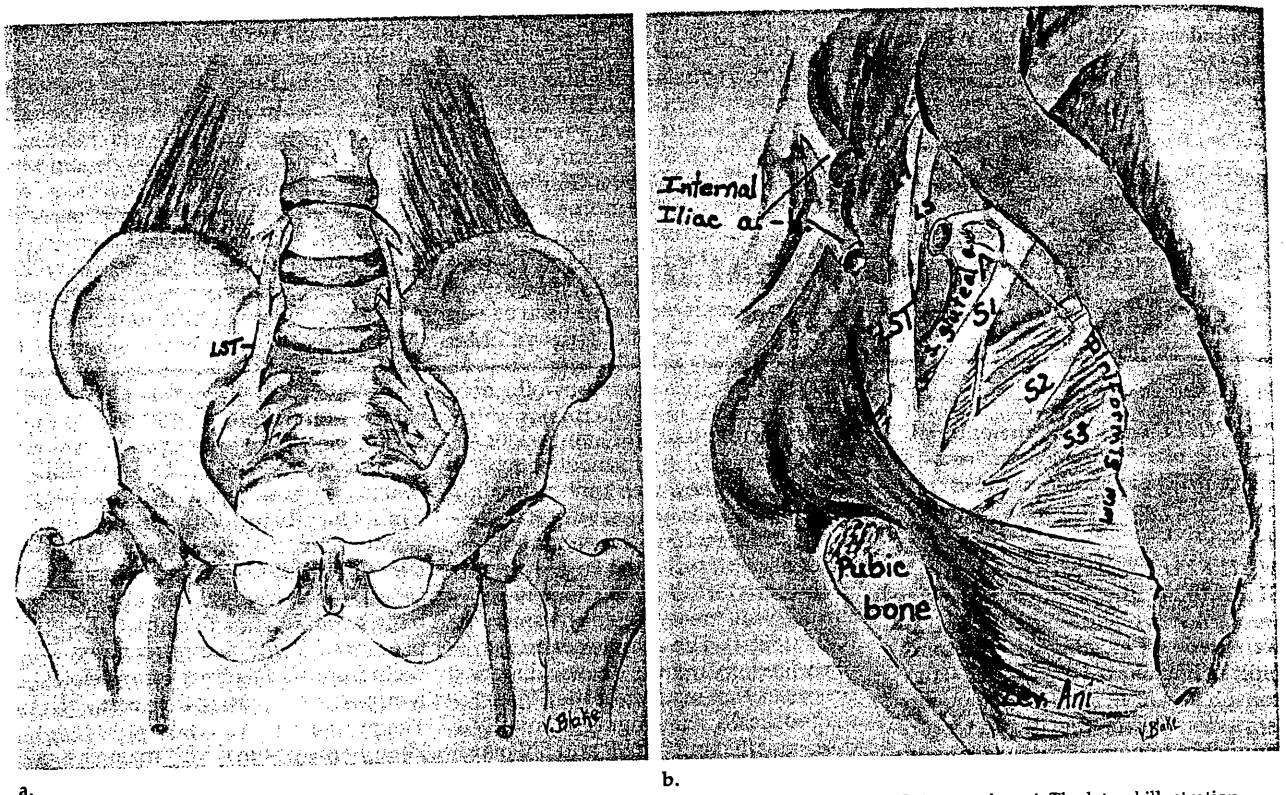

a. b.

Figure 1. Frontal (**a**) and lateral (**b**) illustrations demonstrate the SP, which is formed by the L-4 to S-4 ventral rami. The lateral illustration shows the close relationship between the SP and the ventral surface of the piriformis muscle. The SN exits the pelvis through the GSF. *a.* = artery, *Lev. Ani* = levator ani, *mm* = muscle, *s.* = superior, *v* = vein.

between the internal iliac vessels anteriorly and the piriformis muscle posteriorly and converge at the GSF to form the SN. The piriformis muscle is a key to the relevant anatomy of the SP and functions as an important, easily recognizable landmark for locating the SP and SN. It originates from the anterolateral sacrum from S3-5 and passes through the GSF to insert on the greater trochanter of the femur. The nerve roots that comprise the SP come together on the ventral surface of the piriformis where the proximal SN originates at its inferior margin.

The piriformis muscle divides the SP into three anatomic sections. The preplexal portion of the SP includes the LST and S-1 cranial to the superior border of the piriformis muscle. The plexal segment is that portion of the SP anterior to the piriformis, and the postplexal segment includes the proximal SN caudal to the inferior margin of the muscle and in the GSF.

The SN is the largest nerve in the body, measuring approximately 2 cm in diameter. It contains L-4 to S-3 contributions from the SP. It is formed at the anterior-inferior surface of the piriformis muscle and exits the pelvis through the anterior third of the GSF, posterior to the ischial spine (6). At a slightly more inferior level, the SN is located deep to the gluteal muscles and midway between the ischial tuberosity medially and the greater trochanter of the femur laterally. In the posterior thigh, the SN can be found between the long head of the biceps femoris and the adductor magnus muscles. The SN is actually composed of two large trunks, the common peroneal and tibial nerves, whose fibers do not mix. These nerves are bound together by a common sheath and usually separate above the popliteal fossa into their distinct divisions. The superior gluteal artery—the largest branch of the internal iliac artery—and its accompanying vein exit the pelvis superior to the piriformis muscle. These vessels are often seen in the superiormost aspect of the GSF. Their identity as vessels is confirmed by their tubular appearance and characteristic flow void typical of vessels.

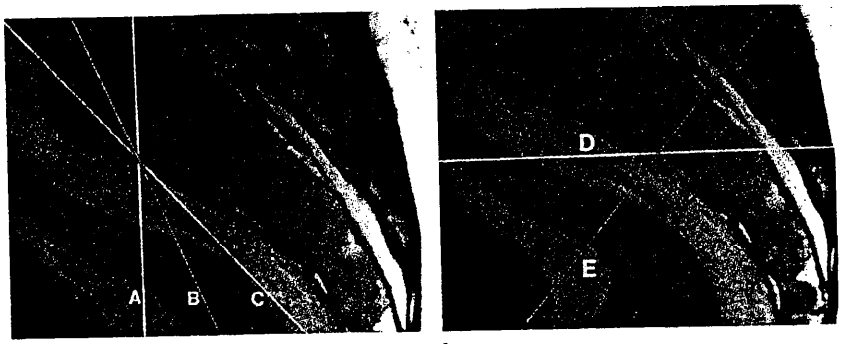

a. b.

Figure 2. Midsagittal MR images demonstrate the (**a**) coronal and (**b**) axial imaging planes studied. The following coronal planes were used: *A* = direct coronal plane parallel to the long axis of the spine, *B* = angled coronal plane midway between the direct coronal and sacral coronal imaging planes, and *C* = sacral coronal plane parallel to the long axis of the sacrum. The following axial planes were used: *D* = direct axial plane perpendicular to the direct coronal plane and *E* = angled axial plane perpendicular to the long axis of the sacrum.

a. b.

Figure 3. Direct coronal images obtained (a) at the level of the sacral promontory and (b) through the GSF. This imaging plane optimally displays the L-4 and L-5 ventral rami, the LST, and the S-1 contribution to the SN. The SN in the GSF is easily demonstrated in b (solid arrows). Note the linear striations in the SN characteristic of peripheral nerves. *A* = levator ani, *SGA* = superior gluteal artery. Open arrows = vessels. Arrowheads in b = superior and inferior boundaries of the GSF.

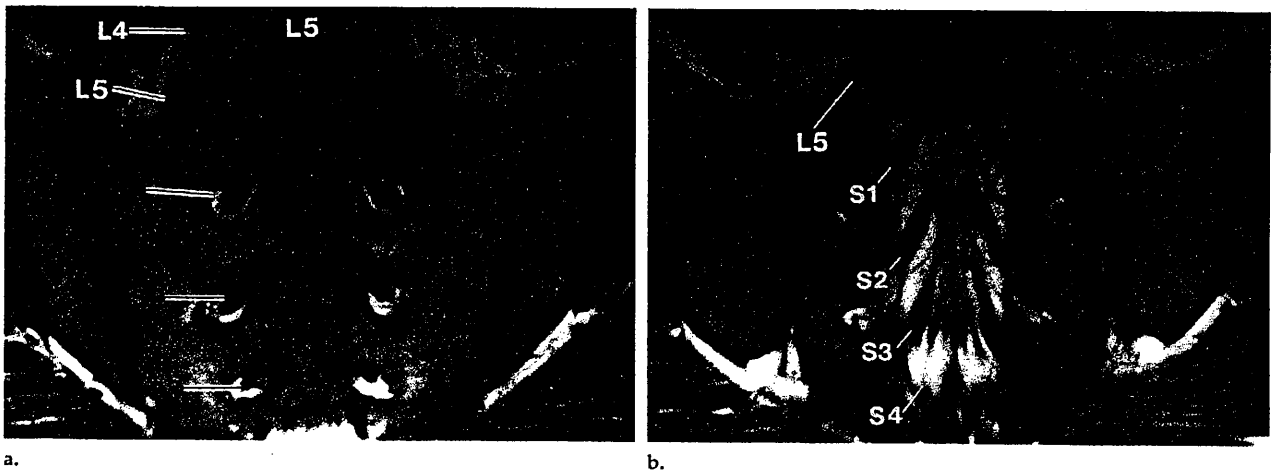

a. b.

Figure 4. Sacral coronal images parallel the long axis of the sacrum and were obtained (a) through the body of the sacrum and (b) through the sacral spinal canal. This is the best plane for evaluating the bony sacrum and the relationship of the sacral foramina to the intraforaminal segments of the S-1 to S-4 ventral rami.

MATERIALS AND METHODS

The SPs of 10 asymptomatic adult volunteers (six men and four women aged 25–36 years) were prospectively imaged. All images were acquired with a 1.5-T MR system (Signa; GE Medical Systems, Milwaukee, Wis). Patients were positioned supine with a pad beneath the knees to decrease lumbar lordosis. Pelvic phased-array surface coils, custom built at this institution, were placed anterior and posterior to the pelvis, using the anterior-superior iliac spine and the ischial tuberosity for the superior and inferior positioning landmarks, respectively.

T1-weighted MR images were obtained by using the following parameters: 600/10 (repetition time msec/echo time msec), two signals acquired, 512 × 384 matrix, 26 × 19–26-cm field of view, and 4-mm-thick sections with a 1-mm intersection gap. Near contiguous sections were utilized to better demonstrate anatomic detail. Phase-encoding direction was anterior to posterior for axial planes and right to left for coronal planes. Spatial radio-frequency pulses placed superior and inferior to the imaging volume were used to diminish blood signal intensity. With this technique, 14–28 images were acquired in each plane of interest with an imaging time of approximately 7 and 14 minutes for single and double acquisitions, respectively.

A total of five imaging planes were used in all patients (Fig 2). These imaging planes included three coronal (Figs 3–5) and two axial (Fig 6) planes. The direct coronal imaging plane was proscribed from a sagittal localizer and was parallel to the longitudinal axis of the lumbar spine. Sacral coronal images were acquired along a line parallel to the longitudinal axis of the sacral spinal canal. The third coronal plane, the angled coronal plane, was midway between the direct and sacral coronal planes. The direct axial and the angled axial imaging planes were perpendicular to the direct and sacral coronal planes, respectively. In addition, imaging was performed in the oblique axial plane (parallel to the piriformis muscle) in five patients (Fig 7).

Two neuroradiologists ranked the conspicuity of individual SP anatomic components, as visualized in each of the imaging planes, by consensus using the following four-grade scoring system: 0 = nerve not visualized, 1 = small portions of nerve visualized, 2 = nerve moderately well visualized, 3 = nerve clearly visualized. The scoring system was applied to structures comprising the SP, including the ventral

rami of L-4, L-5, S-1, S-2, S-3, and S-4 and the LST, which is formed by the union of L-4 and L-5. The ability of each imaging plane to demonstrate the SN in the GSF and the SN in its greatest longitudinal long axis was also evaluated by using the same scale. The SP has an important association with the piriformis muscle, which divides the SP into the following three segments (which were also included in the analysis): the preplexus segment superior to the piriformis, the plexus segment ventral to the piriformis, and the postplexus segment inferior to the piriformis.

An average conspicuity score for the specific anatomic characteristics seen with each of the three coronal and two axial imaging planes was calculated and compared to identify the single best overall coronal and axial imaging planes and to determine which plane was best for identifying anatomic characteristics of the individual SPs. Average conspicuity scores were derived by adding the 10 individual conspicuity scores (one per patient) for each anatomic structure and dividing by 10. The Kruskal-Wallis and Wilcoxon signed rank tests were applied for a formal analysis of statistically significant differences.

RESULTS

Comparison of average conspicuity scores for each of the 12 SP anatomic characteristics evaluated demonstrated that the direct coronal and direct axial planes were the best overall coronal and axial imaging planes for showing the SP (Table). The direct coronal (Fig 3) and direct axial (Fig 6) planes were the most useful for demonstrating the

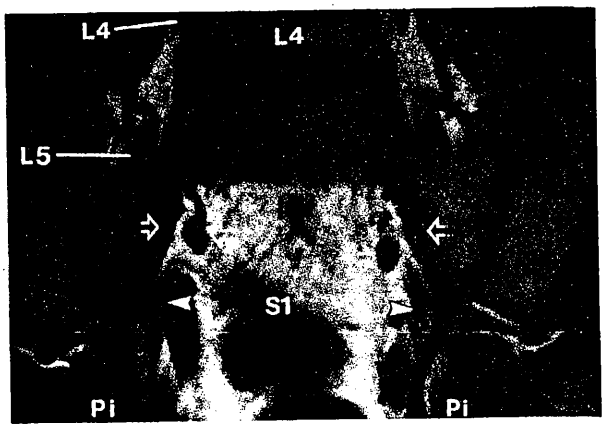

Figure 5. Image obtained in the angled coronal plane, midway between the direct coronal and sacral coronal image planes. Unlike the direct coronal plane, where long segments of the LST and SN are seen, only short segments of nerve roots are identified with the angled coronal plane. *Pi* = piriformis muscle. Arrowheads denote small portions of L-4 to S-1 nerve roots, arrows denote vessels.

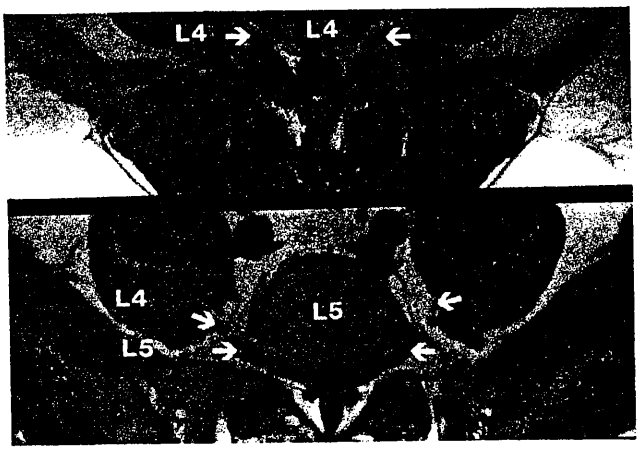

a.

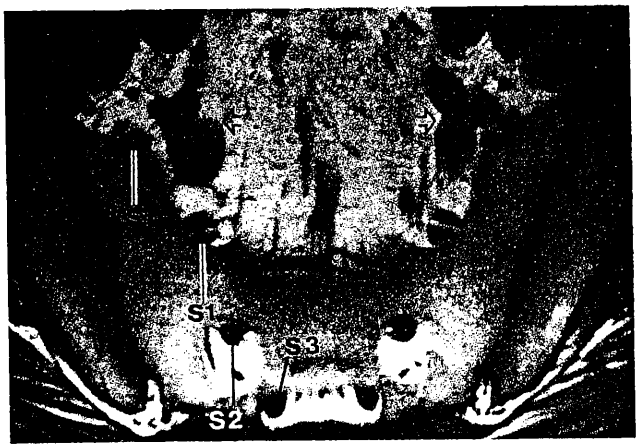

b.

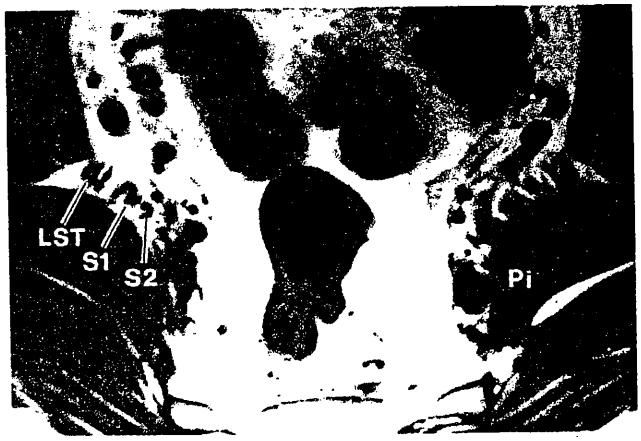

c.

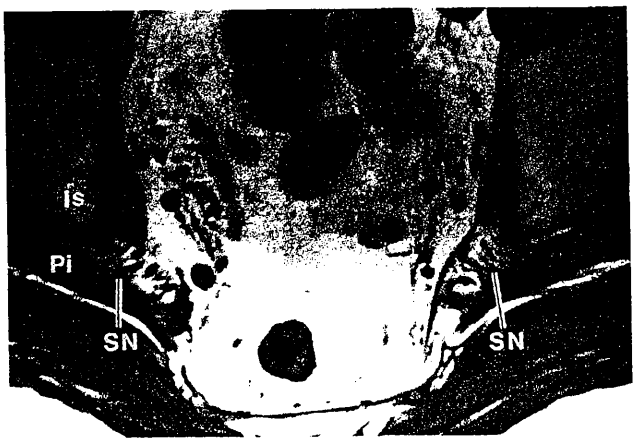

d.

Figure 6. (a–d) Superior (a) to inferior (d) direct axial images. This imaging plane was useful for tracking individual SP nerves on sequential images. Note the fascicular pattern present in the LST and SN in cross section. The LST and S-1 to S-3 ventral rami pass inferiorly, laterally, and posteriorly to join anterior to the piriformis muscle (*Pi*), where the SN is formed. The SN exits the pelvis via the GSF posterior to the ischial spine (*Is*). Arrows in a indicate nerve roots. Arrows in b indicate vascular structures.

L-4 and L-5 ventral rami, the LST, the S-1 contribution to the SN, the SN along its greatest longitudinal length, and the SN in the GSF. The preplexal, plexal, and postplexal sections of the SP were also best evaluated with direct coronal and direct axial planes. The sacral coronal plane (Fig 4) provided the best visualization of the bony sacrum, sacral foramina, and proximal S-1 to S-4 nerve roots. Although not formally evaluated, the sacral coronal plane demonstrated the bony sacrum and sacral foramina well. The best cross-sectional images of the SN were obtained in the direct axial plane (Fig 6). Angled and oblique axial planes did not provide relevant additional information.

Results of the Kruskall-Wallis test comparing direct, axial, and sacral coronal imaging planes demonstrated a P value of .1523, showing no statistically significant difference between any of the coronal imaging planes. Results of the Kruskall-Wallis test comparing direct, angled, and oblique axial imaging planes demonstrated a P value of .0002, showing a statistically significant difference among the axial planes. The Wilcoxon signed rank test was used to determine which (or if all) of the axial plane combinations was statistically different. Comparison of the direct and angled axial planes confirmed the significant difference between these groups found with the Kruskall-Wallis test (P = .0102). Comparison of direct and oblique axial planes (P = .0862) and angled and oblique axial planes (P = .6858) showed no significant difference between these groups.

Conspicuity of Individual Anatomic Components with Each Imaging Plane

Component	Coronal Plane			Axial Plane	
	Direct	Angled	Sacral	Direct	Angled
L-4	3	2.5	2.3	2.9	1.4
L-5	3	2.5	2.7	3	1.8
S-1	3	2.8	2.8	3	2.4
S-2	2.7	2.4	3	3	2.1
S-3	1.7	1.8	3	2.3	1.1
S-4	0.3	0.9	2.7	1.2	0.1
LST	3	2.8	2.6	3	2.2
GSF	3	2.3	1.6	3	2
SN (greatest length)	3	2.1	0.9	1	0.7
Piriformus muscle					
Preplexus segment	3	2.6	2.9	3	2.1
Plexus segment	2.7	2.5	1.9	2.9	2.0
Postplexus segment	2.8	2.1	1.3	2.7	1.3

Note.—Data are the average conspicuity score calculated for each structure in each imaging plane.

DISCUSSION

In addition to being involved with primary diseases of neural origin, the SP may become secondarily involved in a wide variety of pathologic processes originating from pelvic viscera, lymphatic, vascular, or musculoskeletal structures (7,8), resulting in disability and pain. The resulting clinical symptoms and physical examination findings may overlap with those found with abnormalities of the lower lumbar spine (ie, disk herniations). Because of the complex anatomy in this region it may be difficult to precisely locate the level of pathologic involvement by means of clinical history, physical examination, and electrodiagnostic studies alone.

A method of obtaining detailed images of the SP would be useful in the evaluation of the diverse disorders affecting the SP. SP imaging first became possible with the development of high-resolution CT (5). Although CT can be used to identify the major proximal components of the SP, it cannot reliably help distinguish individual peripheral nerves from surrounding pelvic structures with a high degree of certainty. More recently, normal SP anatomy and asso-

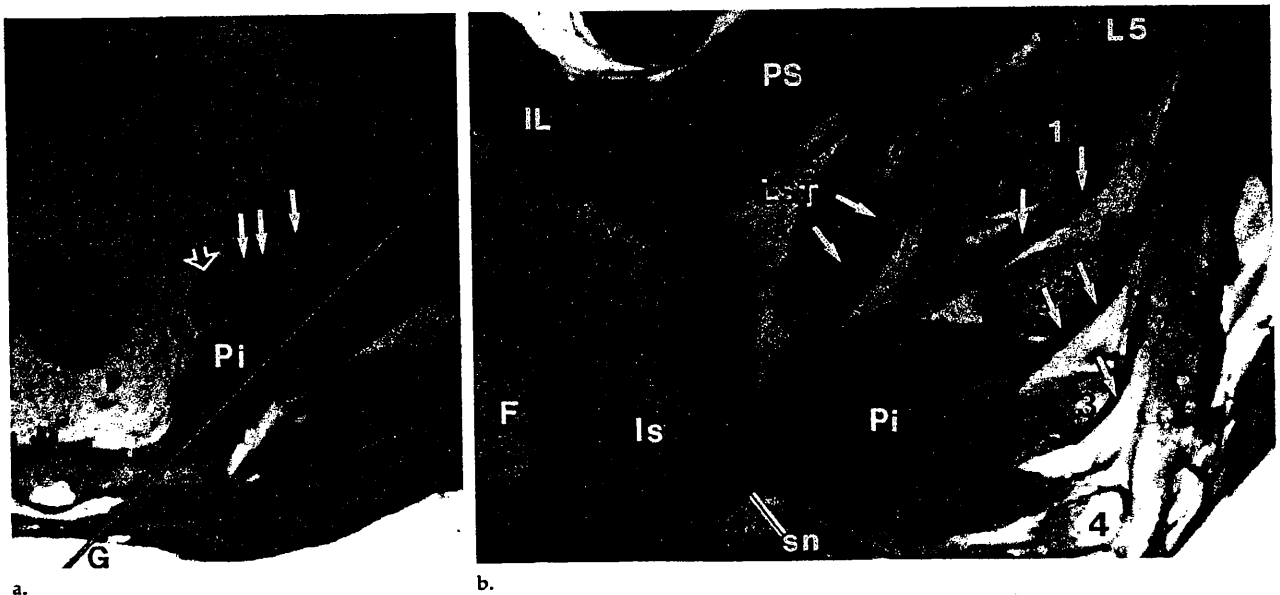

a. b.

Figure 7. (a) Direct axial MR image demonstrates the plane of the oblique axial plane (*G*), which parallels the long axis of the piriformis muscle (*Pi*). The piriformis muscle originates from the anterolateral sacrum and passes through the GSF to insert on the greater trochanter of the femur. Open arrow indicates vessels. Solid arrows indicate the SP. (b) Oblique axial image. The LST and S-1 to S-3 ventral rami are well demonstrated (solid arrows). Note how the LST and the S-1 ventral rami pass anterior to the piriformis muscle (*Pi*) to join the SN posterior to the ischial spine (*Is*). *F* = femoral head, *IL* = iliacus muscle, *PS* = psoas muscle.

ciated abnormalities have been described using MR techniques (9,10). However, these techniques also suffer from the inability to help differentiate small nerve structures from other soft tissues and cannot show the morphologic structure of internal nerves.

MR images acquired with phased-array coils can show detailed SP anatomy and demonstrate the internal structure of peripheral nerves. Phased-array coils acquire image data simultaneously from multiple surface coils. Image data from each coil are combined into a composite image with an improved signal-to-noise ratio. Compared with standard coils, phased-array coils allow acquisition of anatomically detailed images with fewer signals acquired, a smaller field of view, thinner sections, and/or higher-resolution matrices (11).

Peripheral nerves are surrounded by intrapelvic fat and are easily identified by their distinct striated appearance on T1-weighted MR images. This striated appearance is specific for peripheral nerves and thus aids in distinguishing them from surrounding tissues such as blood vessels, lymph nodes, muscle, and adipose tissue (1). The striated pattern seen on MR images can be explained by understanding the histologic microstructure of peripheral nerves.

Peripheral nerves contain multiple thin fascicles that run the length of the nerve. Fascicles are composed of bundles of axons and their Schwann cell coverings, all surrounded by perineurium. Endoneurial fluid bathes the axons within each fascicle. Multiple fascicles are bundled together by a surrounding framework of collagenous and adipose tissue, the external epineurium. Internal epineurium separates individual fascicles within the nerve while external epineurium encircles the entire peripheral nerve complex (12,13).

The striated pattern of peripheral nerves on MR images is due to the longitudinally oriented linear fascicles, which are isointense with muscle at T1-weighted imaging. Individual fascicles are separated from each other by fine linear bands of high signal intensity representing adipose tissue within the internal and external epineurium.

Normal fascicles are long and demonstrate uniform shape and size relative to other fascicles, follow the expected course of the nerve, and are finer and more regular in appearance than striations seen in adjacent muscle. On cross-sectional images, nerve fascicles have a dotlike pattern that is also distinct. In contrast, vascular structures are more anterior, are round or tubular, do not demonstrate a striated pattern, and contain signal void from flowing blood. Muscular striations are short, have variable thickness, and follow the course of the muscle.

High-resolution MR techniques optimize peripheral nerve conspicuity, which allows differentiation of SP nerves from adjacent pelvic viscera, adipose tissue, muscle, and vascular structures. An understanding of internal morphology of normal peripheral nerves aids in the recognition of peripheral nerve abnormalities. We use both the direct coronal and direct axial planes in our routine SP imaging protocol and add additional views as necessary. Alternately, if the specific location of the peripheral nerve abnormality can be determined with clinical history, physical examination, and/or electrodiagnostic studies, the most useful imaging plane for emphasizing the specific SP level can then be selected. ■

Acknowledgments: We thank Valerie Blake for her medical artwork and Betsy Munk for her assistance with the preparation of this manuscript.

References

1. Filler AG, Howe FA, Hayes CE, et al. Magnetic resonance neurography. Lancet 1993; 341:659–661.
2. Filler AG, Howe FA, Winn HR, Howseman AM, Bell BA. Image neurography on standard-gradient MR imagers (abstr). Radiology 1992; 185(P):152.
3. Pech P, Haughton V. A correlative CT and anatomic study of the sciatic nerve. AJR 1985; 144:1037–1041.
4. Lanzieri CF, Hilal SK. Computed tomography of the sacral plexus and sciatic nerve in the greater sciatic foramen. AJR 1984; 143:165–168.
5. Gebarski KS, Gebarski SS, Glazer GM, Samuels BI, Francis IR. The lumbosacral plexus: anatomic-radiologic-pathologic correlation using CT. RadioGraphics 1986; 6:401–425.
6. Gray H; Williams PL, Warwick R, eds. Sacral and coccygeal ventral rami. In: Gray's anatomy of the human body. 36th ed. Philadelphia, Pa: Saunders, 1980; 1110–1117.
7. Cohen BA, Lanzieri CF, Mendelson DS, et al. CT evaluation of the greater sciatic foramen in patients with sciatica. AJNR 1986; 7:337–342.
8. Wetzel LH, Levine E. MR imaging of sacral and presacral lesions. AJR 1990; 154: 771–775.
9. Gierada DS, Erickson SJ, Haughton VM, Estkowski LD, Nowicki BH. MR imaging of the sacral plexus: normal findings. AJR 1993; 160:1059–1065.
10. Gierada DS, Erickson SJ. MR imaging of the sacral plexus: abnormal findings. AJR 1993; 160:1067–1071.
11. Hayes CE, Hattes N, Roemer PB. Volume imaging with MR phased arrays. Magn Reson Med 1991; 18:309–319.
12. Lundberg G, Dahlin LB. Structure and function of peripheral nerve. In: Gelberman RH, ed. Operative nerve repair and reconstruction. Philadelphia, Pa: Lippincott 1991; 3–18.
13. Sunderland S. Terms relating to the structure of nerve fibers and nerve trunks. In: Sunderland S, ed. Nerve injuries and their repair, a critical appraisal. New York, NY: Churchill Livingstone, 1991; 13–16.